

# Magnons in a Quasicrystal: Propagation, Localization and Extinction of Spin Waves in Fibonacci Structures

*Filip Lisiecki,<sup>a</sup> Justyna Rychły,<sup>b,\*</sup> Piotr Kuświk,<sup>a,d</sup> Hubert Głowiński,<sup>a</sup> Jarosław W. Klos,<sup>b,e</sup> Felix Groß,<sup>c</sup> Iuliia Bykova,<sup>c</sup> Markus Weigand,<sup>c</sup> Mateusz Zelent,<sup>b</sup> Eberhard Goering,<sup>c</sup> Gisela Schütz,<sup>c</sup> Maciej Krawczyk,<sup>b</sup> Feliks Stobiecki,<sup>a</sup> Janusz Dubowik,<sup>a</sup> and Joachim Gräfe<sup>c,\*</sup>*

<sup>a</sup>Institute of Molecular Physics, Polish Academy of Sciences, M. Smoluchowskiego 17, 60-179  
Poznań, Poland

<sup>b</sup>Faculty of Physics, Adam Mickiewicz University, Umultowska 85, 61-614 Poznań, Poland

<sup>c</sup>Max Planck Institute for Intelligent Systems, Heisenbergstraße 3, 70569 Stuttgart, Germany

<sup>d</sup>Centre for Advanced Technology, Adam Mickiewicz University, Umultowska 89c, 61-614  
Poznań, Poland

<sup>e</sup>Institute of Physics, University of Greifswald, Felix-Hausdorff-Str. 6, 17489 Greifswald,  
Germany

## **Abstract**

Magnonic quasicrystals exceed the possibilities of spin wave (SW) manipulation offered by regular magnonic crystals, because of their more complex SW spectra with fractal characteristics. Here, we report the direct x-ray microscopic observation of propagating SWs in a magnonic quasicrystal, consisting of dipolarly coupled permalloy nanowires arranged in a one-dimensional Fibonacci sequence. SWs from the first and second band as well as evanescent waves from the band gap between them are imaged. Moreover, additional mini-band gaps in the spectrum are demonstrated, directly indicating an influence of the quasiperiodicity of the system. The experimental results are interpreted using numerical calculations and we deduce a simple model to estimate the frequency position of the magnonic gaps in quasiperiodic structures. The demonstrated features of SW spectra in one-dimensional magnonic quasicrystals allows utilizing this class of metamaterials for magnonics and makes them an ideal basis for future applications.

## **1. Introduction**

Magnonic crystals are periodically modulated magnetic structures, which enable tailoring of the magnonic band structure and formation of allowed and forbidden bands in the spin wave (SW) spectrum.<sup>1,2</sup> Additionally, the SW spectrum can easily be modified by an external magnetic field or a change of the magnetization configuration in the structure.<sup>3</sup> This offers fine tuning and re-programmability,<sup>4</sup> which are desirable properties for potential applications.<sup>5</sup> Apart from periodic modulations, defects in the regular structure can also alter SW propagation. Defects can cause the appearance of localized SW modes with their amplitude confined to the disturbed area. Equally, they can introduce additional magnonic branches at frequencies inside the band gaps of

the SW spectrum.<sup>6-9</sup> In a periodically arranged array of magnetic stripes, a stripe with differing dimensions can be considered and designed as such a defect. Thereby, providing an opportunity for the design of cavity resonators and ultra-narrow band filters.<sup>10,11</sup>

Quasicrystals, unlike crystals, do not have periodicity albeit possessing long-range order, which results in a discrete diffraction pattern.<sup>12</sup> They are characterized by more complex dispersion relations than those of periodic systems with an increased number of forbidden band gaps and narrow allowed bands. Spectra of quasicrystals also include localized excitations concentrated in various parts of the self-similar structure, which is a characteristic feature of such aperiodic systems.<sup>13</sup> Previously, these properties have been widely studied in the context of photonics and phononics for one-dimensional (1D) quasicrystals designed by using the Fibonacci sequence.<sup>14-16</sup>

Quasiperiodicity has also been applied to magnonic systems.<sup>17-28</sup> Fundamental theoretical studies used Fibonacci structures comprised of multilayers<sup>17-21</sup> or bi-component stripes<sup>22,23</sup> to investigate the spectrum of exchange or dipolar SWs respectively. However, these hypothetical structures were far from experimental realization. First experimental realizations of quasiperiodicity in magnonics were based on grooves in a micrometer thick YIG film.<sup>24</sup> All electrical spin wave spectroscopy measurements indicated an influence of the quasiperiodicity on the SW spectrum.<sup>24</sup> A key experimental realization of flexible magnonic quasicrystals were 2D arrays of Py nanobars in Penrose, Ammann, or Fibonacci arrangement.<sup>25-28</sup> However, these studies were focused on the magnetization reversal processes and only demonstrated a rich ferromagnetic resonance (FMR) spectrum of these systems, hinting at a more complex SW band structure.<sup>24-28</sup> So far, there has been no study of the microscopic behavior, propagation, nor localization of SWs in magnonic quasicrystals.

Here, we present the direct microscopic observation of propagating SWs in a 1D quasiperiodic magnonic structure formed by thin Py stripes arranged in a Fibonacci sequence. This is achieved by using scanning transmission X-ray microscopy (STXM) that provides ultimate spatial ( $<20$  nm) and temporal ( $<50$  ps) resolution. Propagating modes from the first and second bands were detected with a band gap between them. Furthermore, the existence of a mini-band gap within the first band was demonstrated, showing the influence of the quasiperiodicity on the dispersion relation. We complement the experimental results with calculations that show good agreement with the resonant frequencies and profiles of the investigated modes and allow their interpretation. Moreover, we propose a simple model based on diffraction structure factor calculations, which allows to predict the frequency positions of most magnonic bandgaps in the SW spectra of 1D magnonic quasicrystals.

## 2. Methods and theory

### 2.1. Sample characteristics

Nanowires (NWs, length  $L = 10 \mu\text{m}$ ) were fabricated by e-beam lithography and subsequent lift-off in a thin Py film ( $\text{Ni}_{80}\text{Fe}_{20}$ , thickness  $d = 30$  nm) on a  $\text{Si}_3\text{N}_4(100 \text{ nm})/\text{Si}$  substrate with membrane windows for X-ray transmission measurements.  $100 \mu\text{m}$  wide arrays of narrow ( $W_{\text{N}} = 700$  nm) and wide ( $W_{\text{W}} = 2W_{\text{N}} = 1400$  nm) NWs were arranged quasiperiodically using Fibonacci's inflation rule. According to this rule, a sequence of higher order  $n$  is determined by the sum of the two previous structures ( $S_n = S_{n-1} + S_{n-2}$ ) as shown in Fig. 1a. To ensure magnetostatic coupling between the NWs an air gap ( $W_{\text{G}} = 80$  nm) was introduced between adjacent NWs.<sup>29</sup>

For SW excitation a coplanar waveguide (CPW) made from Cu(150 nm)/Al(10 nm) with a 2  $\mu\text{m}$  wide signal line was fabricated on top of the structure using direct laser lithography<sup>30</sup> and a lift-off technique. The CPW lines are aligned along the NWs axis to excite a dynamic magnetic field with a component perpendicular to the array ( $x$ -axis). Additionally, a static magnetic field  $H_{\text{app}}$  was applied parallel to the NWs axis ( $y$ -axis). A sketch of the sample geometry superimposed with an exemplary STXM result, indicating SW propagation across the NW array, is shown in Fig. 1b.

Time-resolved STXM measurements were conducted at the MPI IS operated MAXYMUS end station at the UE46-PGM2 beam line at the BESSY II synchrotron radiation facility. The samples were illuminated under perpendicular incidence by circularly polarized light in an applied in-plane field of up to 240 mT that was generated by a set of four rotatable permanent magnets.<sup>31</sup> The photon energy was set to the absorption maximum of the Fe L3 edge to get optimal XMCD contrast for imaging. A lock-in like detection scheme allows sample excitation at arbitrary frequencies at a time resolution of 50 ps using all photons emitted by the synchrotron.

## 2.2. Numerical calculations

To calculate SW spectra we solve the Landau-Lifshitz (LL) equation:

$$\frac{\partial \mathbf{M}(\mathbf{r}, t)}{\partial t} = \mu_0 \gamma \mathbf{M}(\mathbf{r}, t) \times \mathbf{H}_{\text{eff}}(\mathbf{r}, t), \quad (1)$$

where  $t$  is time and  $\mathbf{r}$  is the position vector. Damping has been neglected in the calculations.

$\mathbf{H}_{\text{eff}}(\mathbf{r}, t)$  is an effective magnetic field, which is assumed to be the sum of three terms:

$\mathbf{H}_{\text{eff}}(\mathbf{r}, t) = \mathbf{H}_0 + \mathbf{H}_{\text{ex}}(\mathbf{r}, t) + \mathbf{H}_{\text{dm}}(\mathbf{r}, t)$ .  $\mathbf{H}_{\text{ex}}(\mathbf{r}, t)$  is an exchange field and  $\mathbf{H}_{\text{dm}}(\mathbf{r}, t)$  is a dynamic demagnetizing field with components along the  $x$  and  $y$  directions (due to the assumed

geometry the static demagnetizing field is 0). The  $\mathbf{H}_{\text{ex}}(\mathbf{r}, t)$  and  $\mathbf{H}_{\text{dm}}(\mathbf{r}, t)$  fields are defined in Ref. <sup>32</sup>.

From Eq. (1) we find the dynamical components of the magnetization  $\mathbf{m}(\mathbf{r}, t)$  where  $\mathbf{M}(\mathbf{r}, t) = M_z(\mathbf{r})\hat{\mathbf{e}}_z + \mathbf{m}(\mathbf{r}, t)$ . We use a linear approximation, *i.e.* we neglect the higher order terms arising in Eq. (1) with respect to  $\mathbf{m}$ . This is justified when  $M_z$  is assumed to be constant in time, namely when  $|\mathbf{m}(\mathbf{r}, t)| \ll M_z(\mathbf{r})$ , and therefore  $M_z \approx M_S$ , where  $M_S$  is saturation magnetization. We seek solutions of the LL Eq. (1) in the form of monochromatic SWs, having harmonic dynamics in time:  $e^{2\pi if t}$ , where  $f$  is the frequency of the SW. Eq. (1) is complemented with the Maxwell equations to determine the demagnetizing fields. With these equations we define the eigenvalue problem, which is solved by using a FEM approach with COMSOL 5.1 to obtain the dispersion relation and profiles of the SWs. For more details concerning this computation, we refer to Ref. <sup>33</sup>. In numerical calculation we used  $M_S = 0.76 \times 10^6$  A/m, the exchange constant  $A = 1.3 \times 10^{-11}$  J/m, and gyromagnetic ratio  $\gamma = 1.76 \times 10^{11}$  rad/sT for Py.

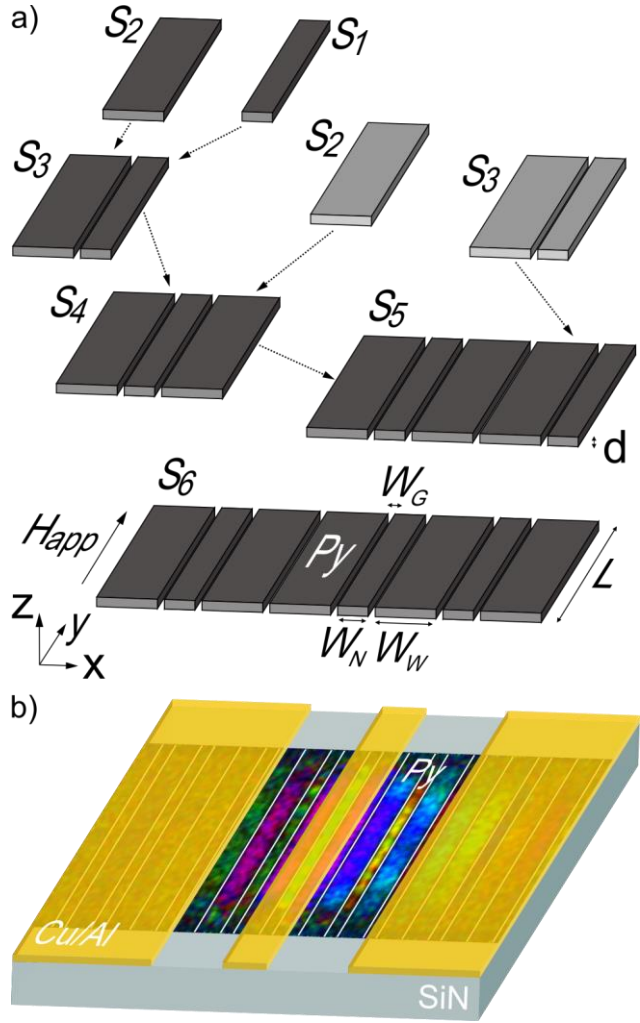


**Fig. 1** (a) Arrangement of the first sequences ( $S_1$  to  $S_6$ ) of Fibonacci structures consisting of Py NWs separated by air gaps. (b) Sample scheme with CPW (yellow) used for SW excitation and superimposed an exemplary STXM result.

### 3. Results and discussion

**3.1. Propagating spin waves in the structure.** Time-resolved STXM measurements with continuous wave excitation from the CPW were conducted in the frequency range from 3.6 to 6.6 GHz (*cf.* Fig. 3). Magnetization dynamics from select resonances (A-F) in an applied static field of  $H_{\text{app}} = 5$  mT are shown in Fig. 2a. In these images, the SW amplitude is indicated as brightness and the relative SW phase as color (*cf.* Fig. 2b). Additionally, the static Fibonacci structure (light gray) with the CPW (dark gray) are shown in Fig. 2c.

For all frequencies where SWs could be excited, a gradual variation of the phase along the propagation direction is visible in the measurements. This indicates that the SWs in the Fibonacci structure exhibit a propagating character. For 3.8 GHz (mode A in Fig. 2a) and 4.2 GHz (mode B), SW modes with strong amplitude are visible. For 4.6 GHz (marked C), however, we observed no excitation of SWs in the sample, indicating that an additional mini-band gap opens in the SW spectrum at this frequency. This agrees with our numerical calculations (as will be discussed in the further part) and is characteristic for waves in quasicrystals, as the spectrum is much more complex and can feature additional band gaps in comparison to the analogous periodic structure. At higher frequencies (modes D-F) we again observe SW excitation. For 4.9 GHz (mode D) and 5.1 GHz (mode E) SWs are visible again, but at a much weaker amplitude that decays rapidly with distance from the signal line. However, for even higher frequencies, *i.e.* 5.7 GHz (mode F), there is again a strong signal for SW excitation. In the higher frequency band (modes D-F) the phase varies over a shorter distance, indicating a smaller wavelength of the excited SWs.

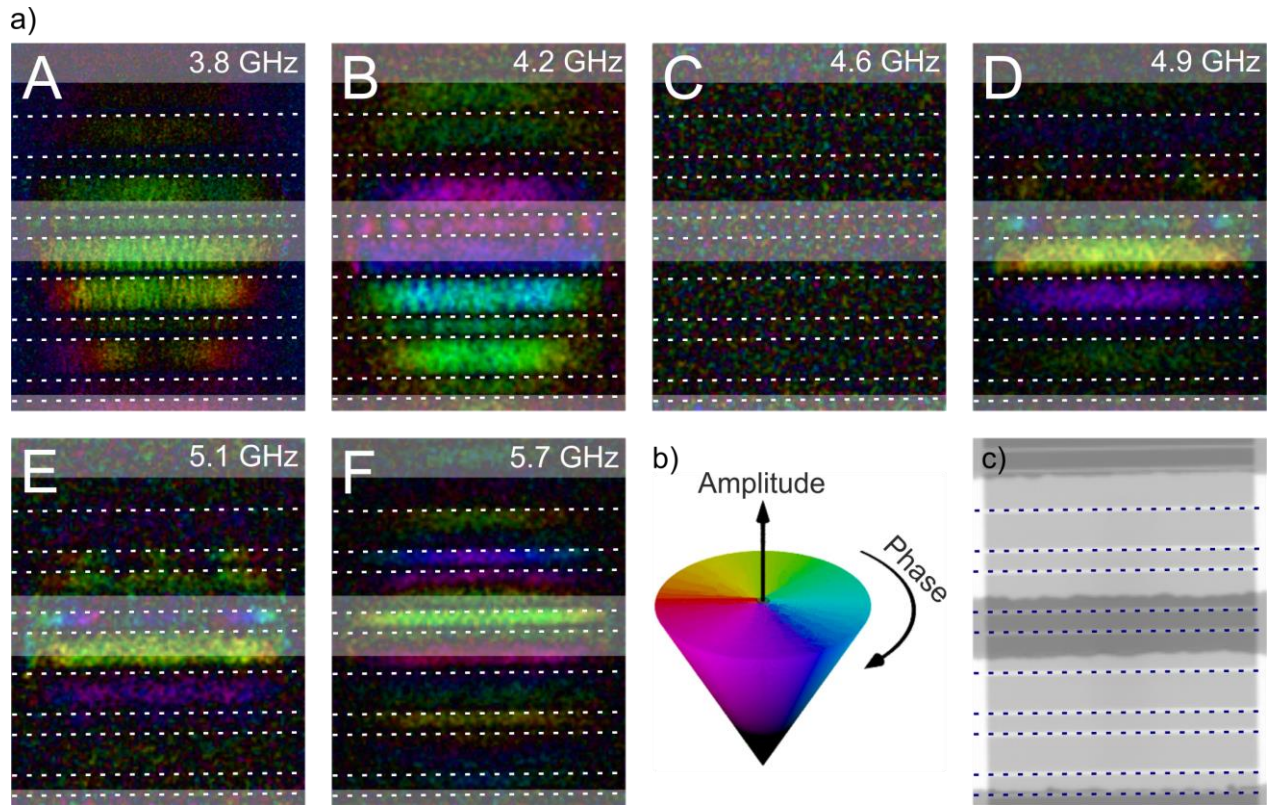


**Fig. 2** (a) SW amplitude and phase for different excitation frequencies at 5 mT. The transparent gray rectangles mark the position of the CPW and the dashed white lines the gaps between the stripes. (b) Legend for SW amplitude (brightness) and phase (color). (c) Static image of the Fibonacci structure (light gray) with the signal line (dark gray) near the center of the image, and the ground lines at the top and bottom edges of the image (dark gray). See Supporting Information for the videos.

From the measurements, we are able to estimate the decay length ( $\Lambda$ ) of SWs propagating through the structure, it is from an exponential fit of the spatial amplitude distribution according to  $A \exp(-x/\Lambda)$ , where  $A$  is the SW amplitude and  $x$  is the distance from the excitation source. We

calculated the decay length to be  $\lambda = 14 \pm 2 \text{ } \mu\text{m}$ , which is in good agreement with the literature value for Py waveguides.<sup>34</sup>

To aid interpretation of the experimental results, we solved the linearized Landau-Lifshitz (LL) equation complemented by the magnetostatic Maxwell equations in the frequency domain, using a finite element method (FEM) approach as described earlier. Thereby, we obtained the resonance frequencies and amplitude distributions of the standing SW oscillations in the system. In the calculations we assumed an array of infinitely long Py NWs, keeping the thickness, widths and the Fibonacci arrangement (*cf.* Fig. 1a) from the experiment. The total size of the structure, *i.e.* the number of NWs, in the calculations is also close to the experimental sample. For the  $S_{11}$  Fibonacci sequence the total width of all elements, *i.e.* the array size in the  $x$ -direction, is  $108 \text{ } \mu\text{m}$  compared to  $100 \text{ } \mu\text{m}$  for the experimental sample.

The calculated frequencies of the SW excitations are shown in Fig. 3a as full red dots. The horizontal axis in Fig. 3a shows the solution number, indicating the assumed order of SW excitations. We are showing the first 100 solutions with the lowest frequencies. The spectrum starts at 3.6 GHz, which is significantly above the FMR frequency of 1.9 GHz for Py. This significant upshift can be attributed to the dipolar pinning of SWs<sup>35</sup> on the interfaces of the ferromagnetic stripes that are separated by air gaps. In the spectrum (*cf.* Fig. 3a), we can distinguish a wide band gap between 5.0 and 5.8 GHz, splitting the spectrum into two parts, *i.e.* the two main bands. Below this gap there are 55 solutions, which is equal to the number of wider NWs (of width  $W_w$ ) in the whole simulated structure. This is a characteristic feature for solutions of the eigenvalue problem for a wave equation in finite systems and exists for periodic structures as well. As opposed to crystals, in quasicrystals, a number of mini-gaps additionally splits each band. The existence of such mini-gaps (indicated by gray horizontal bars in Fig. 3a) is a direct

consequence of the long-range quasiperiodic order of Py NWs coupled by magnetostatic stray fields.

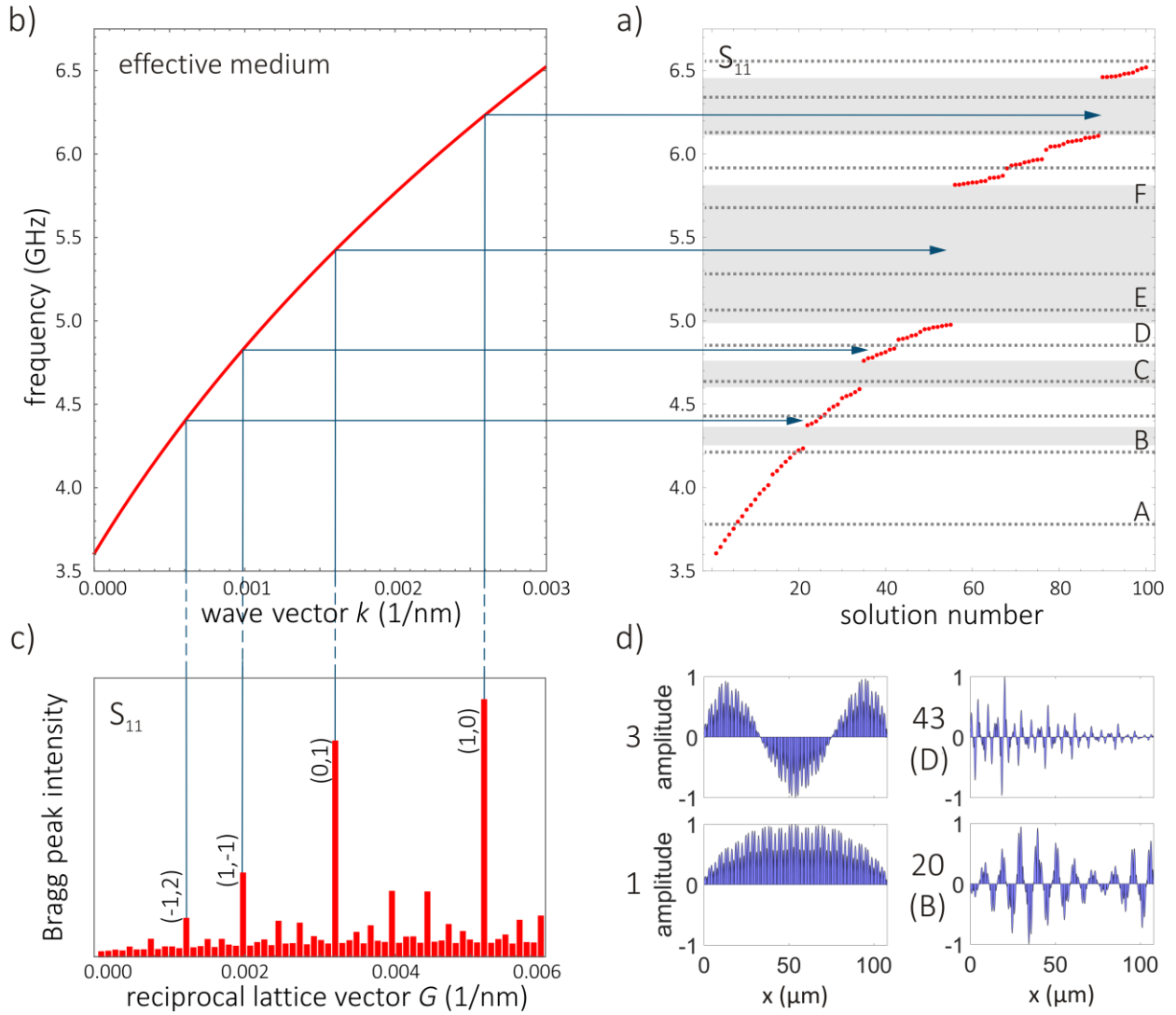


**Fig. 3** Results of the numerical calculations: (a) the SW spectrum for the planar magnonic quasicrystal is compared to (b) the analytical SW dispersion in a homogeneous plain film with effective material parameters. In subfigure (a) the frequencies of the eigenmodes of the  $S_{11}$  Fibonacci sequence (*cf.* Fig. 1) are sorted in ascending order (solid red dots). The magnonic gaps are marked as gray areas and the horizontal dashed lines indicate the frequencies at which the experimental measurements have been performed. The horizontal lines marked A to F indicate

the modes presented in Fig. 2. (c) The Fourier spectrum of the spatially dependent material parameter (e.g.  $M_S$ ) calculated for the considered  $S_{11}$  sequence. The reciprocal lattice vectors  $G$  of the Fourier components determine the SW's wave vectors  $k$  for which the Bragg condition ( $G/2 = k$ ) is fulfilled. The blue arrows in (c), (b), (a) link the: (c) reciprocal lattice vectors  $G$  (corresponding to the Bragg peaks of highest intensity) to the (b) frequencies of the SWs in the effective medium, which then point at the largest magnonic gaps of the Fibonacci quasicrystal. The integer numbers in brackets over the highest Bragg peaks at (c) are the pairs of indexes for reciprocal vectors (*cf.* Eq. 3) of the Fibonacci quasicrystal. At (d) the amplitude and phase distributions of the selected modes are shown. The modes with solution number 20 and 43 are compared with the measured modes B and D respectively.

To allow a direct comparison of the numerical solutions and the experimental results, and to identify the band gaps, the experimentally measured frequencies are indicated by dashed horizontal lines in Fig. 3a. It is clear that modes A and B fall into the lower band, explaining the long wavelengths of propagating SWs shown in Fig. 2a. Mode C lies in the mini-gap within the first band, thus, SW propagation is prohibited, corresponding to the weak SW amplitude measured in STXM at this frequency. For mode D, SW propagation is recovered as it occurs at a frequency within the band. Mode E falls in the wide main bandgap, which separates the first and the second band. At this frequency, only forced excitation can be observed, which is the reason for the strong decay of SW amplitude when moving away from the excitation source. Modes of even higher frequency, *e.g.* mode F, lie already above the main gap and originate from the second band. These will be discussed elsewhere.

For selected modes, the spatial distributions of the SW amplitude and phase are shown in Fig. 3d. The low-frequency excitations are standing waves distributed throughout the whole simulated structure, whereas the number of nodes (points with a change of the sign of the phase) increases with frequency. The mode at the lowest frequency does not have any change of the phase sign, the second mode has one nodal line in the middle of the structure, and so on (see the envelope of the first and third solutions presented in Fig. 3d). At higher frequencies the envelope of the SWs becomes irregular with several maxima located in different parts of the structure, as shown in Fig. 3d for solution number 20 and 43 corresponding to modes B and D respectively. Nevertheless, up to a frequency of 5.0 GHz the standing waves are solely formed from fundamental oscillations of single NWs, *i.e.* without nodal points inside NWs. This property justifies grouping of these modes into one main band. Thus, the last mode (solution number 55) in the first band has antiphase oscillations in neighboring wide NWs (*cf.* Fig. 4). The second band, starting at 5.8 GHz (solution number 58), continues the harmonic oscillation series with irregular envelopes, but all of the excitations from this band feature a nodal line within the wide NWs, an indicative property of SWs from this band.

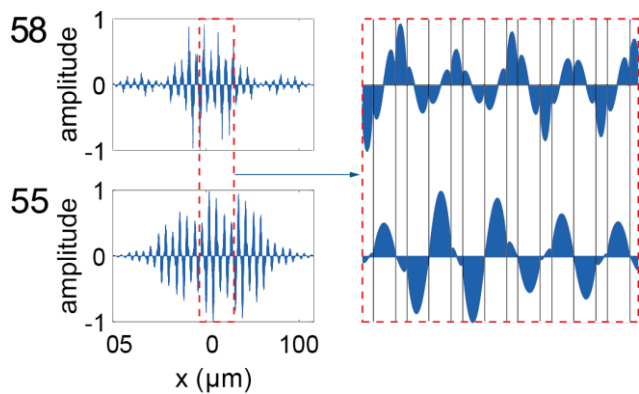


**Fig. 4** Amplitude and phase distribution for solution number 55 and 58, *i.e.* the last mode of the first band and the first mode of the second band respectively (left panel). And enlargement of the

central part (right panel, enclosed by red dashes) with solid grey lines marking the air gaps between the stripes. By this, we can compare how the amplitude and the phase are distributed through the wide and narrow stripes in the first band, and in the second band.

In Fig. 5 a comparison between the calculated and experimental out-of-plane magnetization component ( $m_z$ ) is shown for selected modes. The calculated results are superimposed as a red line on the experimental values shown as blue bars. Calculated profiles were adjusted to account for exponential SWs decay, *i.e.* the decay of the SW amplitude envelope with increasing distance from the signal line. In STXM measurements propagating SWs were detected, thus,  $m_z$  changes in time ( $t$ ) and space ( $x$ ). In Fig. 5 the magnetization profile for an arbitrary time slice  $t_0$  is shown. For the lowest measured frequency in the first band (mode A), the sign of  $m_z$  in all NWs is the same, except for the outmost visible stripes, which means that half of the wavelength is almost as long as the measurement window and about 10  $\mu\text{m}$ . As expected, for higher frequencies shorter waves are excited. For modes B and D, half of the wavelength is observed to be 5  $\mu\text{m}$  and 2.2  $\mu\text{m}$  respectively. As mentioned earlier, mode F belongs to the second band with  $\sim 2.2 \mu\text{m}$  as half of the wavelength, however, the sign of  $m_z$  changes across the wide stripes as the phase of the SW oscillation changes. Overall, the results of the calculations match the measured data very well, validating our interpretation.

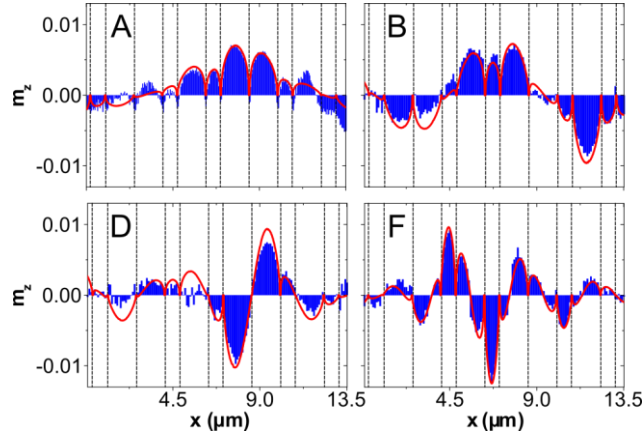


**Fig. 5** Calculated (red solid lines) and experimental profiles (blue bars) of selected SW modes. Vertical dashed lines indicate the positions of the air gaps between the Py NWs in the structure.

**3.2. Estimation of the band gaps and mini-gaps positions.** In the SW spectrum presented in Fig. 3a, we have distinguished two main bands separated by a wide band gap between 5.0 and 5.8 GHz, and a set of mini-band gaps of much smaller widths, both types were confirmed by STXM measurements. The formation of these gaps can be related to the Bragg scattering of SWs with wavenumbers fulfilling the Bragg condition. Thus, the location of the reciprocal lattice numbers  $G$  in the wave vector space should give us information about the position of the frequency gaps and mini-gaps in the spectrum.

For a wave with wavenumber  $k$ , the Bragg condition may be written as:

$$G(h_1, h_2)/2 = k, \quad (2)$$

where  $h_1$  and  $h_2$  are integer numbers. The 1D reciprocal lattice vectors  $G(h_1, h_2)$  are defined for the Fibonacci lattice as:<sup>36,37</sup>

$$G(h_1, h_2) = \frac{2\pi}{a} \left( h_1 + \frac{1}{\phi} h_2 \right), \quad (3)$$

where:

$$\bar{a} = \frac{\varphi(W_W+W_G)+(W_N+W_G)}{\varphi+1} \quad (4)$$

is an averaged period of the Fibonacci structure, and  $\varphi = \frac{1+\sqrt{5}}{2}$  is the so called *golden ratio*. The 1D reciprocal lattice numbers (3) are indexed by two integer numbers  $h_1$  and  $h_2$ . To explain this we recall that the Fibonacci sequence can be formed by the projection of a square lattice to a straight line tilted at an irrational angle  $\alpha$ , where  $\tan(\alpha) = 1/\varphi$ . The projection is done from the stripe parallel to the mentioned line<sup>37</sup>. To obtain the reciprocal lattice vectors (3) for the corresponding quasiperiodic sequence of lattice nodes, obtained from the projection to the line inclined at an angle  $\alpha$ , the Fourier transform of a square lattice (set of Dirac delta peaks) and the Fourier transform of the stripes (*sinc* function) have to be convoluted<sup>37</sup>. Note that for 1D Fibonacci structures, the reciprocal lattice vectors are densely packed numbers in 1D reciprocal space, due to the irrational factor  $1/\varphi$  in Eq. (3). The wide gap is related to the Bragg scattering of SWs at the smaller reciprocal number  $G$  ( $h_1 = 0, h_2 = 1$ ). For the Py NW Fibonacci structure considered here,  $\bar{a} = 1212.6$  nm and the main Bragg resonance condition (2) is fulfilled for  $k = 1.6 \mu\text{m}^{-1}$ , which is close to the wavenumber of the experimentally detected SWs for one of the first modes from the second band at the edge of the main gap ( $1.42 \mu\text{m}^{-1}$  for the 5.7 GHz, mode F). The gaps of smaller width are indicated by reciprocal lattice numbers  $G$  determined by other values of indices  $h_1$  and  $h_2$ .

To predict the position of the gap frequencies in 1D quasicrystals we need to project the wavenumbers found from Eq. (2) onto the dispersion relation of SWs. Therefore we propose to use the dispersion relation of a homogeneous ferromagnetic film with effective parameters. The measured and calculated SW profiles (Fig. 5) show a strong reduction of the dynamic components of the magnetization amplitude close to the edges of the NWs. This proves a

significant dynamical demagnetizing effect, induced by the presence of NW edges, which leads to pinning of the dynamical magnetization and to an increase of the FMR frequency. Thus, the FMR frequency for the patterned magnetic system considered here with an in-plane shape anisotropy can be expressed with the demagnetizing factors  $N_d$  and  $1 - N_d$  (which take values from 0 to 1):<sup>38</sup>

$$f_{\text{FMR}} = \frac{1}{2\pi} \sqrt{(\omega_0 + N_d \omega_M)(\omega_0 + (1 - N_d) \omega_M)}, \quad (5)$$

where  $\omega_0 = \gamma \mu_0 H_{\text{app}}$  and  $\omega_M = \gamma \mu_0 M_S$  are characteristic frequencies corresponding to the applied field and the saturation magnetization (expressed in frequency units) respectively.

$\mu_0$  and  $\gamma$  are the magnetic permeability of vacuum and the gyromagnetic ratio respectively. For the same parameters as in the numerical simulations, we were able to shift the FMR frequency  $f_{\text{FMR}}$  (5) to the value obtained in numerical calculations (3.6 GHz) by fitting the demagnetizing factor  $N_d$ . The relatively small value of  $N_d = 0.0157$  ensures the required upshift of  $f_{\text{FMR}}$ .

The dispersion relation for the homogeneous film with effective material parameters and in-plane demagnetizing effects can be calculated according to:

$$f(k) = \frac{1}{2\pi} \sqrt{(\omega_0 + \omega_M \lambda^2 k^2 + N_d \omega_M)(\omega_0 + \omega_M \lambda^2 k^2 + (N_d - 1) \omega_M) + \omega_M^2 / 4(1 - e^{-2kd})}, \quad (6)$$

with the exchange length  $\lambda = \sqrt{\frac{2A}{\mu_0 M_S^2}} = 6.19$  nm for Py. Using the dispersion relation (6), we estimate the maximum value of the wavenumber  $k_{\text{max}} = 0.0035$  nm<sup>-1</sup> for the frequency range up to 6.5 GHz considered in numerical calculations. The obtained dispersion relation is shown in Fig. 3b. By projecting the wavenumbers fulfilling the Bragg condition (2) on the dispersion relation  $f(k)$  we are able to determine the expected positions of the band gaps.

Apart from the frequencies for which gaps open, we can also estimate the relative widths of these gaps. This can be done with the help of the diffraction spectra of the structure. The diffraction properties of any kind of structure are given by the structure factor  $F(G)$  which can be estimated by Fourier transform of the spatial dependence of the material parameter, *e.g.* the saturation magnetization  $M_S$ , in the composite systems. We calculated the discrete Fourier transform of  $M_S$ :

$$F(G_l) \propto \sum_{j=0}^{N-1} M_S(x_j) e^{-iG_l x_j}, \quad (7)$$

where  $x_j = L \frac{j}{N}$  is the location of  $M_S(x_j)$  in the sample in real space and  $G_l = \frac{2\pi}{L} l$  is the discretized reciprocal lattice number. The modulus  $|F(G_l)|$  obtained for the structure considered here is presented in Fig. 3c. The height of the bars representing  $|F(G_l)|$  is related to the intensity of the Bragg peaks of the scattered waves. The location  $G_l$  of Bragg peaks with large intensity corresponds to the frequency gaps opened at  $f_{\text{gap}}$  given by  $k(f_{\text{gap}}) = G_l/2$ , for which the relation  $k(f)$  can be found from the dispersion relation (6). The position of the highest peaks from the numerically calculated Fourier spectrum of the quasiperiodic structure strictly coincides with the wavenumbers fulfilling the analytical formula (3).

The procedure described above allowed us to connect the structure of the magnonic quasicrystal with the frequency gaps in the SW spectrum, which are in good agreement with the results of the numerical calculations and experimental data obtained from STXM measurements.

#### 4. Conclusion

We have experimentally observed propagating SWs in real space and time domain in 1D Fibonacci quasicrystals of dipolarly coupled Py NWs of two different sizes and fully recovered

and explained this system using numerical calculations. Thereby, we have demonstrated the existence of propagating SW modes in such quasicrystals, crucial for future magnonic data processing applications. We have shown that SW propagation is not restricted to the long-wavelength limit, for which the structure can be considered as an effective medium, but also occurs at higher frequencies, for which the structure's long-range quasiperiodic order is critical. Additionally, we have experimentally proven the existence of mini-band gaps that are a direct consequence of the collective SW effects in magnonic quasicrystals. Furthermore, a simple analytical method has been derived for the estimation of the magnonic gaps and mini-gaps in the SW spectra of 1D quasicrystals, providing a powerful tool for designing quasiperiodic systems.

The mini-gaps are wide enough to prohibit propagation of SWs despite the finite SW damping, thus, offering usefulness for potential applications in the filtering of microwave signals. Moreover, these propagating SWs in quasicrystal structures featuring mini-gaps originating from a dense spectrum of diffraction peaks in reciprocal space, offering unprecedented flexibility in the design of effective non-linear processes,<sup>39</sup> which is one of the main challenges in the application of magnonics to transfer and process information.<sup>40</sup>

## **Acknowledgments**

The study has received funding from European Union's Horizon 2020 research and innovation programme under the Marie Skłodowska-Curie GA No644348 (MagIC). Helmholtz Zentrum Berlin / BESSY II is gratefully acknowledged for allocating beam time at the MAXYMUS end station. J.W.K. would like to acknowledge the support of the Foundation of Alfred Krupp Kolleg Greifswald and the National Science Centre of Poland Grant No.: UMO-2016/21/B/ST3/00452.

J.R. would like to acknowledge the financial support from the Adam Mickiewicz University Foundation and from the National Science Centre of Poland under ETIUDA grant number UMO-2017/24/T/ST3/00173.

### **Author Contributions**

F.L. and P.K. designed and prepared the samples. F.L., H.G., F.G., I.B., M.W. and J.G. performed measurements. J.R., J.W.K., M.Z. and M.K. developed the theory. J.G., E.G., G.S., M.K., F.S., J.D. managed the study. F.L., J.R., J.W.K., M.K. and J.G. wrote the manuscript. All authors discussed the results and manuscript.

### **Additional Informations**

Electronic supplementary information (ESI) available.

**Competing financial interests:** The authors declare no competing financial interest.

### **Corresponding authors**

\*E-mail: rychly@amu.edu.pl (J.R.)

\*E-mail: graefe@is.mpg.de (J.G.)

### **ORCID**

**Filip Lisiecki:** 0000-0002-9292-4942

**Justyna Rychly:** 0000-0003-3630-114X

**Jarosław W Kłos:** 0000-0002-5858-2950

**Joachim Gräfe:** 0000-0002-4597-5923

### **References**

1 M. Krawczyk and D. Grundler, *J. Phys. Condens. Matter*, 2014, **26**, 123202.

- 2 R. L. Stamps, S. Breitzkreutz, J. Åkerman, A. V. Chumak, Y. Otani, G. E. W. Bauer, J.-U. Thiele, M. Bowen, S. A. Majetich, M. Kläui, I. L. Prejbeanu, B. Dieny, N. M. Dempsey and B. Hillebrands, *J. Phys. Appl. Phys.*, 2014, **47**, 333001.
- 3 S. Tacchi, M. Madami, G. Gubbiotti, G. Carlotti, S. Goolaup, A. O. Adeyeye, N. Singh and M. P. Kostylev, *Phys. Rev. B*, 2010, **82**, 184408.
- 4 J. Topp, D. Heitmann, M. P. Kostylev and D. Grundler, *Phys. Rev. Lett.*, 2010, **104**, 207205.
- 5 A. V. Chumak, V. I. Vasyuchka, A. A. Serga and B. Hillebrands, *Nat. Phys.*, 2015, **11**, 453–461.
- 6 K. Di, V. L. Zhang, M. H. Kuok, H. S. Lim, S. C. Ng, K. Narayanapillai and H. Yang, *Phys. Rev. B*, 2014, **90**, 060405.
- 7 J. Rychły and J. W. Kłos, *J. Phys. Appl. Phys.*, 2017, **50**, 164004.
- 8 V. V. Kruglyak, M. L. Sokolovskii, V. S. Tkachenko and A. N. Kuchko, *J. Appl. Phys.*, 2006, **99**, 08C906.
- 9 J. W. Kłos and V. S. Tkachenko, *J. Appl. Phys.*, 2013, **113**, 133907.
- 10 V. L. Zhang, H. S. Lim, S. C. Ng, M. H. Kuok, X. Zhou and A. O. Adeyeye, *AIP Adv.*, 2016, **6**, 115106.
- 11 Y. Filimonov, E. Pavlov, S. Vystostkii and S. Nikitov, *Appl. Phys. Lett.*, 2012, **101**, 242408.
- 12 H. Jagodzinski, *Z. Für Krist.*, 1991, **196**, 1–19.
- 13 F. Capolino, Ed., *Metamaterials Handbook—Theory and Phenomena of Metamaterials*, CRS Press, Boca Raton, London, New York, 2009.
- 14 E. Maciá, *Appl. Phys. Lett.*, 1998, **73**, 3330–3332.
- 15 S. Golmohammadi, M. K. Moravvej-Farshi, A. Rostami and A. Zarifkar, *Opt. Express*, 2007, **15**, 10520–10532.
- 16 S. M. Lubin, A. J. Hryn, M. D. Huntington, C. J. Engel and T. W. Odom, *ACS Nano*, 2013, **7**, 11035–11042.
- 17 C. H. O. Costa, M. S. Vasconcelos and E. L. Albuquerque, *J. Appl. Phys.*, 2011, **109**, 07D319.
- 18 I. P. Coelho, M. S. Vasconcelos and C. G. Bezerra, *J. Magn. Magn. Mater.*, 2011, **323**, 3162–3167.
- 19 C. H. O. Costa and M. S. Vasconcelos, *J. Phys. Condens. Matter*, 2013, **25**, 286002.
- 20 I. P. Coelho, M. S. Vasconcelos and C. G. Bezerra, *Solid State Commun.*, 2010, **150**, 1760–1765.
- 21 L. D. Machado, C. G. Bezerra, M. A. Correa, C. Chesman, J. E. Pearson and A. Hoffmann, *J. Appl. Phys.*, 2013, **113**, 17C102.
- 22 J. Rychły, J. W. Kłos, M. Mruczkiewicz and M. Krawczyk, *Phys. Rev. B*, 2015, **92**, 054414.
- 23 J. Rychły, J. W. Kłos and M. Krawczyk, *J. Phys. Appl. Phys.*, 2016, **49**, 175001.
- 24 S. V. Grishin, E. N. Beginin, Y. P. Sharaevskii and S. A. Nikitov, *Appl. Phys. Lett.*, 2013, **103**, 022408.
- 25 V. S. Bhat, J. Sklenar, B. Farmer, J. Woods, J. T. Hastings, S. J. Lee, J. B. Ketterson and L. E. De Long, *Phys. Rev. Lett.*, 2013, **111**, 077201.
- 26 V. S. Bhat, J. Sklenar, B. Farmer, J. Woods, J. B. Ketterson, J. T. Hastings and L. E. De Long, *J. Appl. Phys.*, 2014, **115**, 17C502.
- 27 B. Farmer, V. S. Bhat, J. Sklenar, E. Teipel, J. Woods, J. B. Ketterson, J. T. Hastings and L. E. De Long, *J. Appl. Phys.*, 2015, **117**, 17B714.
- 28 S. Choudhury, S. Barman, Y. Otani and A. Barman, *ACS Nano*, 2017, **11**, 8814–8821.
- 29 J. Topp, D. Heitmann and D. Grundler, *Phys. Rev. B*, 2009, **80**, 174421.

- 30 W. Koczorowski, P. Kuświk, M. Przychodnia, K. Wiesner, S. El-Ahmar, M. Szybowicz, M. Nowicki, W. Strupiński and R. Czajka, *Mater. Sci. Semicond. Process.*, 2017, **67**, 92–97.
- 31 D. Nolle, M. Weigand, P. Audehm, E. Goering, U. Wiesemann, C. Wolter, E. Nolle and G. Schütz, *Rev. Sci. Instrum.*, 2012, **83**, 046112.
- 32 M. Mruczkiewicz, M. Krawczyk, V. K. Sakharov, Y. V. Khivintsev, Y. A. Filimonov and S. A. Nikitov, *J. Appl. Phys.*, 2013, **113**, 093908.
- 33 A. G. Gurevich and G. A. Melkov, *Magnetization Oscillations and Waves*, CRC Press, Boca Raton, 1996.
- 34 K. Sekiguchi, T. N. Vader, K. Yamada, S. Fukami, N. Ishiwata, S. M. Seo, S. W. Lee, K. J. Lee and T. Ono, *Appl. Phys. Lett.*, 2012, **100**, 132411.
- 35 K. Y. Guslienko, S. O. Demokritov, B. Hillebrands and A. N. Slavin, *Phys. Rev. B*, 2002, **66**, 132402.
- 36 M. F. Limonov and R. M. De La Rue, *Optical Properties of Photonic Structures. Interplay of Order and Disorder*, CRC Press, BocaRaton, 2012.
- 37 C. Janot, *Quasicrystals*, Oxford University Press, Oxford, UK, 2012.
- 38 D. Stancil and A. Prabhakar, *Spin Waves Theory and Applications*, Springer US, Boston, MA, 2009.
- 39 K. Fradkin-Kashi, A. Arie, P. Urenski and G. Rosenman, *Phys. Rev. Lett.*, 2001, **88**, 023903.
- 40 A. V. Chumak, A. A. Serga and B. Hillebrands, *Nat. Commun.*, 2014, **5**, 4700.